# A Lectin-Based Gold Nanoparticle Assay for Probing Glycosylation of Glycoproteins[†]

*Germarie Sánchez-Pomales, Todd A. Morris, James B. Falabella, Michael J. Tarlov and Rebecca A. Zangmeister**

Bioprocess Measurements Group, Biochemical Science Division, National Institute of Standards and Technology, 100 Bureau Drive., MS 8362, Gaithersburg, MD 20899-8362
*rebecca.zangmeister@nist.gov; telephone: 301-975-4912; fax: 301-975-2643

[†] This article contains supplementary material available from the authors upon request or via the Internet at http://wileylibrary.com.

ABSTRACT. We report a glycoanalysis method in which lectins are used to probe the glycans of therapeutic glycoproteins that are adsorbed on gold nanoparticles. A model mannose-presenting glycoprotein, ribonuclease B (RNase B), and the therapeutic monoclonal antibody (mAb) rituximab, were found to adsorb spontaneously and non-specifically to bare gold nanoparticles such that glycans were accessible for lectin binding. Addition of a multivalent binding lectin, such as concanavalin A (Con A), to a solution of the modified gold nanoparticles resulted in cross-linking of the nanoparticles. This phenomenon was evidenced within 1 minute by a change in the hydrodynamic diameter, $D_H$, measured by dynamic light scattering (DLS) and a shift and increase in absorbance of the plasmon resonance band of the gold nanoparticles. By combining the sugar-binding specificity and the cross-linking capabilities of lectins, the non-specific adsorption of glycoproteins to gold surfaces, and the unique optical reporting properties of gold nanoparticles, a glycosylation pattern of rituximab could be generated. This assay provides advantages over currently used glycoanalysis methods in terms of short analysis time, simplicity of the conjugation method, convenience of simple spectroscopic detection, and feasibility of providing glycan characterization of the protein drug product by using a variety of binding lectins.

KEYWORDS. glycoprotein, antibody, lectin, gold nanoparticle, glycan, assay

## INTRODUCTION

The majority of approved protein therapeutics are glycosylated (Walsh and Jefferis 2006). Glycosylation is the enzymatic linking of sugar molecules to produce oligosaccharides, also known as glycans, covalently attached to the protein. This process can result in significant heterogeneity in the composition and structure of attached glycans (Brooks 2009; Jefferis 2005). This pattern of glycosylation is crucial in biopharmaceutical development and manufacturing because it can influence binding, clearance, immunogenicity, and mechanism of action of the

protein therapeutic (Rudd et al. 2001; van Kooyk and Rabinovich 2008). Therefore, the glycan profile of the protein must be carefully monitored to ensure compliance to quality control standards and claims (Chirino and Mire-Sluis 2004; Jefferis 2005; Schneider 2008; Walsh and Jefferis 2006). Currently, glycan profiles are most commonly determined by enzymatic cleavage of the glycans from the protein followed by chromatographic (Kamoda and Kakehi 2006; Rudd et al. 1994) or mass spectrometric characterization (Dell and Morris 2001; Kawasaki et al. 1999; Lim et al. 2008; Zamfir and Peter-Katalinic 2004). Although these methods provide rigorous characterization of glycan structure, they can be time consuming, require expert interpretation, and are not suitable for monitoring glycan profile changes during a production run in a manufacturing facility. In contrast, lectin based assays hold promise as a simple, inexpensive, and rapid alternative for glycosylation screening of protein drugs and for clinical diagnostic applications (Blow 2009; Chen et al. 2007; Hirabayashi 2008; Hwang et al. 2008; Kuno et al. 2005). The need for rapid glycosylation screening methods and advances in this area of research have been recently reviewed (Cunningham et al. 2010).

In this paper, we present a simple glycosylation assay based on the detection of nanoparticle aggregates due to lectin binding to sugar groups present on a glycoprotein directly adsorbed to gold nanoparticles. Gold nanoparticles have been extensively studied for assay applications due to the sensitivity of their surface plasmon absorption band to the size, aspect ratio, and composition of the particles and the refractive index of their immediate environment (Liz-Marzán 2006). Assays have been developed based on color changes caused by the adsorption of an analyte to the bare gold nanoparticle surface (Morris et al. 2002; Mulvaney 1996; Sardar et al. 2009) or by modifying the nanoparticles with analyte specific affinity ligands (Elghanian et al. 1997; Schofield et al. 2006). Multivalent interactions with the analyte can induce cross-linking

of the nanoparticles which in turn causes aggregation and a color change due to coupling of the surface plasmons (Kaur et al. 2007; Medley et al. 2008; Schofield et al. 2006). This approach has been most often used to develop colorimetric assays for detecting metal ions (Liu and Lu 2004; Obare et al. 2002; Si et al. 2007), DNA hybridization events (Cho et al. 2008; Elghanian et al. 1997; Storhoff et al. 1998), protein-protein binding (Nam et al. 2003; Tessier et al. 2008; Thanh and Rosenzweig 2002), and protein-carbohydrate interactions (Dai et al. 2006; Fromell et al. 2005; Gao et al. 2008; Kim et al. 2009; Liang et al. 2009; Wang et al. 2010; Watanabe et al. 2010).

Recently, Huo *et al.* reported highly sensitive detection and accurate analysis of cancer biomarkers in a one-step homogeneous immunoassay using gold nanoparticle probes and detection by dynamic light scattering (DLS) analysis (Liu et al. 2008). Gold nanoparticles have a large scattering cross section in the surface plasmon resonance wavelength region allowing the size distribution of the gold nanoparticle probes to be monitored by DLS. This approach has also been applied to biomolecular binding studies (Jans et al. 2009) and the detection of small molecules (Dasary et al.; Yang et al. 2011). In related studies, carbohydrate-functionalized surfactant vesicle nanoparticles have been shown to be a model platform for the study of lectin carbohydrate interactions (Thomas et al. 2009). Thomas *et al.* monitored the aggregation behaviour of glucose-functionalized surfactant vesicles with the addition of Con A and reported binding kinetics and a binding site separation distance for Con A commensurate with literature values using this platform.

Assays based on lectin-induced cross-linking of modified gold nanoparticles (Au NPs) have been reported for the detection of lectins by Au NPs conjugated with monosaccharide-terminated small molecules (Schofield et al. 2007; Schofield et al. 2006; Toyoshima and Miura 2009) and

the interrogation of protein-carbohydrate interactions (Dai et al. 2006; Fromell et al. 2005; Kim et al. 2009; Liang et al. 2009; Wang et al. 2010; Watanabe et al. 2010). To our knowledge, the work described here is the first demonstration of a direct lectin-based nanoparticle assay for screening of oligosaccharides of glycoproteins, where changes in the nanoparticles size distribution and optical properties of the glycoprotein-modified Au NPs are analyzed.

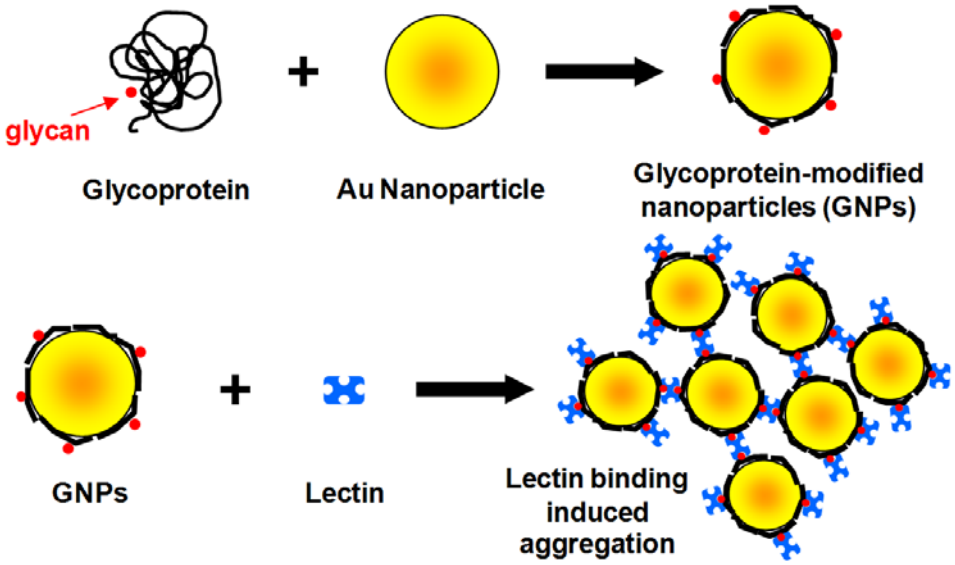


Scheme 1. Schematic representation of the rapid glycan assay.

The strategy for detecting intact glycan sugars on glycoproteins directly bound to gold nanoparticles using lectins via nanoparticle aggregation is depicted in Scheme 1. A key feature of the approach is to first adsorb the glycoprotein to the nanoparticle surface. We hypothesize that adsorption of glycoproteins to bare gold nanoparticle surfaces promotes protein unfolding and presentation of the relatively hydrophilic oligosaccharides to the surrounding aqueous solution, a condition likely to be favorable for glycan-lectin interactions (Hwang et al. 2008). Subsequent introduction of a multivalent lectin with affinity for the glycan of the glycoprotein will result in binding to the glycoprotein-modified nanoparticle followed by cross-linking of the nanoparticle, thereby causing changes in the scattering efficiency and optical properties of the

sol. In contrast, introduction of a lectin with little or no affinity for the glycoprotein oligosaccharides is expected to produce no significant change in the colloidal suspension.

We demonstrate proof-of-concept of the assay using a model high mannose glycoprotein RNase B and apply it to the therapeutic monoclonal antibody (mAb) rituximab, which is used to treat autoimmune disorders and blood cancers. The interaction of lectins with glycoprotein-modified gold nanoparticles was monitored using DLS and UV-visible absorbance measurements. X-ray photoelectron spectroscopy (XPS), analytical ultracentrifugation (AUC), and matrix-assisted laser desorption/ionization time of flight mass spectral analysis (MALDI TOF MS) were also used to characterize the glycoprotein-modified nanoparticles.

## MATERIALS AND METHODS[1]

### *Materials*

Con A, wheat germ agglutinin (WGA), peanut agglutinin (PNA), and Jacalin lectins were purchased from Vector Laboratories (Burlingame, CA, USA) and used without further purification. Ribonuclease A (RNase A, from bovine pancreas, reagent grade), ribonuclease B (RNase B, from bovine pancreas, >80 %), bovine serum albumin, sodium chloride (99.9 %), manganese chloride tetrahydrate (99.99 %), calcium chloride dihydrate (98 %), 4-(2-hydroxyethyl)piperazine-1-ethanesulfonic acid (HEPES, 99.5 %), and indium foil (99.99 %) were purchased from Sigma-Aldrich (St. Louis, MO, USA) and used as received. Inhibitory

[1] Certain commercial equipment, instruments, or materials are identified in this document. Such identification is not intended to imply recommendation or endorsement by the National Institute of Standards and Technology, nor is it intended to imply that the products identified are necessarily the best available for the purpose.

sugars, D-mannose (99.9%, Calbiochem), D-(+)-glucose (99.5%, Sigma), and N-acetylglucosamine (99%, Sigma) were used as received. Sodium borate decahydrate, ACS grade, was obtained from Fisher Scientific (Pittsburgh, PA, USA). Sodium chloride (99.9%) and potassium carbonate anhydrous, ACS grade, were purchased from Mallinckrodt Baker. Citrate-stabilized gold nanoparticles (average diameter 10 nm, 5.7 x $10^{12}$ particles/mL, and 30 nm, 2.0 x $10^{11}$ particles/mL) were purchased from Ted Pella (Redding, CA, USA).

The mAb rituximab was purchased from RxUSA using a prescription. Its formulation consists of 10 mg/mL of the antibody, 9 mg/mL of sodium chloride, 7.35 mg/mL of sodium citrate dihydrate, and 0.7 mg/mL polysorbate 80 at pH = 6.5. The formulated rituximab was purified by protein A affinity chromatography. The purified rituximab, with a concentration of ~9 mg/mL, was stored at −18 ºC in 25 mmol/L phosphate buffer, pH 7.4, with 0.01% $NaN_3$. Type I water (UV treated; 18 MΩ·cm; 0.2 micrometer final filter) was used for all solution preparations. A microcentrifuge with a fixed angle rotor (Eppendorf model 5415 D) was used for preparative centrifugation.

*Dynamic light scattering analyses*

DLS measurements were made with a Malvern Zetasizer Nano ZS DLS system at 25˚C. Approximately 200 µL of sample were added to low-volume disposable cuvettes and allowed to equilibrate for thirty seconds before analysis. Ten runs of ten seconds each were used to analyze each sample. All particle sizes (hydrodynamic diameters, $D_H$) reported here were based on intensity distributions and were obtained using the non-negative least squares analysis method. The hydrodynamic diameter values reported represent the average and the standard deviation of at least three measurements. A detection angle of 173° was used for the analyses.

*UV-visible absorption analyses*

UV-visible absorption spectra were made with a Perkin-Elmer spectrophotometer (Lambda Bio 20) using a 1 cm path length quartz cuvette. The absorption spectrum was measured from 950 nm to 450 nm at a scan rate of 240 nm/min and a step size of 1 nm against a water or buffer background sample.

*RNase B-gold nanoparticle conjugation*

To prepare RNase B-modified gold nanoparticles, RNase B was first dissolved in water at a concentration of 1 mg/mL, a stock concentration that was determined to result in saturation of protein coverage by AUC analysis as discussed in the Supplementary Information. The pH of the as-received 10 nm gold nanoparticle solution was raised to ≈ 10 with 0.1 mol/L NaOH, as measured by EMD colorpHast pH test strips (EMD Millipore, San Diego, CA, USA). Protein solution was added to the gold nanoparticle solution at a volume ratio of 1:10; the final protein concentration is therefore 100 µg/mL when mixed with the nanoparticles. The solution was mixed and allowed to incubate at room temperature for at least 30 min. Then it was centrifuged at 13 200 r/min for 40 min, and the supernatant containing excess RNase B was decanted and replaced with water.

*Rituximab-gold nanoparticles conjugation*

Rituximab-Au NP conjugates were prepared by adding 334 µL of pH adjusted ( ≈ 10 with 0.1 mol/L NaOH) 30 nm Au NPs (~200 pmole/L) to 6 µL of 9 mg/mL purified rituximab and 160 µL of Type I water. The dispersion was allowed to interact for 1 minute at room temperature using an automatic shaker. The dispersion was then centrifuged for 10 minutes at 10 000 r/min. After centrifugation, the supernatant was decanted, and the rituximab-Au NP conjugates were

redispersed in water to a final sample volume of 500 µL. A fresh batch of rituximab-Au NP conjugates was prepared before each experiment.

*Flocculation tests*

We performed flocculation tests for the rituximab-Au NP conjugates in order to determine the minimum amount of rituximab needed to stabilize the conjugates against salt-induced flocculation. One hundred microliters of 30 nm Au NPs (≈200 pmol/L) were added to different volumes of rituximab and diluted to a final volume of 130 µL with nanopure water. The AuNPs and rituximab were allowed to interact for 1 minute at room temperature under continuous mixing using an automatic shaker. Afterwards, 20 µL of 10% NaCl by mass was added to each sample. After 5 minutes of interaction with NaCl, we analyzed the samples by UV-visible spectroscopy and DLS. We used the results of these tests to select the concentration of rituximab to be used for subsequent experiments.

*Lectin-induced aggregation of the RNase B-Au NP conjugates*

Stock lectin solutions were made by dissolving 1 mg of lectin in 1 mL of HEPES buffered saline, HBS (pH 7.4, 0.15 mol/L NaCl, 0.01 mol/L HEPES, 1 mmol/L $Ca^{2+}$, 1 mmol/L $Mn^{2+}$). Con A requires trace amounts of $Ca^{2+}$ and $Mn^{2+}$ as co-factors for activity. A final lectin concentration of 50 µg/mL was obtained by dilution of the stock lectin solution in a ratio of 1:20 (v/v) with the RNase B gold nanoparticle solution. DLS and UV-visible spectroscopy were used to analyze the samples.

*Lectin-induced aggregation of the rituximab-Au NP conjugates*

WGA, PNA and Jacalin lectin solutions were prepared at a concentration of 60 µg/mL in 0.0025 mol/L sodium tetraborate buffer with 0.0015 mol/L NaCl (pH = 7.5). Aqueous Con A solutions were prepared at a concentration of 60 µg/mL in the presence of 1 mmol/L $Ca^{2+}$ and

$Mn^{2+}$. For the lectin-based colorimetric assay, equal volumes of rituximab-Au NP conjugates and lectin were mixed and allowed to interact for up to two hours at room temperature with the aid of an automatic shaker. The final lectin concentration was 30 μg/mL. The samples were analyzed by UV-visible spectroscopy and DLS.

## RESULTS AND DISCUSSION

### *Characterization of RNase B-modified gold nanoparticles*

The model glycoprotein RNase B was first examined to demonstrate the lectin-based gold nanoparticle glycan assay. RNase B possesses N-linked saccharide structure of $-(GlcNac)_2Man_x$ where GlcNAc is N-acetylglucosamine, Man is α-mannose and x is 5 to 9 (Fu et al. 1994; Tarelli et al. 2000). Although nine compositionally- or structurally-distinct glycoforms are present in commercially-available RNase B, all glycoforms possess α-mannose moieties on the non-reducing end. The oligosaccharide portion of RNase B constitutes approximately 10 % of the ≈ 14.7 kDa protein. Therefore, we expect RNase B-modified gold nanoparticles to present α-mannose moieties at a relatively high surface density.

The size distribution of the RNase B-modified gold nanoparticles was determined using DLS. The hydrodynamic diameter of the gold nanoparticles as measured by DLS increased from (17.9 ± 0.5) nm before RNase B adsorption to (21.3 nm ± 0.7) nm after conjugation with RNase B (Figure S-1). This increase in hydrodynamic radius of ≈ 1.7 nm agrees well with a reported average diameter of 1.7 nm for RNase A measured by DLS (Zhang et al. 2011). UV-visible absorbance analysis was also used to evaluate the conjugation of RNase B to the gold nanoparticles. Unmodified 10 nm gold colloids exhibit a characteristic $\lambda_{max}$ absorbance peak at 520 nm due to the surface plasmon resonance of the colloidal gold, whereas the $\lambda_{max}$ value of

RNase B-modified gold colloids shifted to 525 nm (data not shown). The 5-nm red shift is likely due to changes in the refractive index at the gold nanoparticle surface and is consistent with those reported for the adsorption of proteins to colloidal gold (Brewer et al. 2005; Lacerda et al. 2009; Liu et al. 2009; Thobhani et al.).

In addition to the size and optical changes associated with RNase B adsorption, results from XPS and =AUC provided similar evidence for the adsorption of RNase B to the gold nanoparticles. A minimum concentration of 0.1 mg/mL RNase B was required to form a stable suspension of the modified Au NPs, as determined from AUC data. Details of the instrumentation and results obtained by these methods are presented and discussed in greater detail in the Supplementary Information (Sections III and IV).

*Glycoanalysis of RNase B by Gold Nanoparticles*

The interaction of the lectin Con A with the RNase B-modified gold nanoparticles was examined because it binds specifically to the sugars glucose and mannose. The interaction of Con A with the mannose moieties of RNase B has been well-studied (Kuno et al. 2005; Sparbier et al. 2005). For the solution conditions used in these experiments (pH 7.4), Con A exists as a tetramer with four independent sugar binding sites (Zand et al. 1971).

To demonstrate that the specific binding of the lectin causes the observed change in surface plasmon resonance, two non-mannose specific lectins, peanut agglutinin (PNA) and wheat germ agglutinin (WGA), were also introduced to the RNase B-modified gold nanoparticles in separate control experiments. PNA and WGA are multivalent lectins specific for ß-D-galactose(1-3)-D-N-acetylgalactosamine (Loris et al. 1998) and N-acetylglucosamine (Rini 1995) respectively. Because PNA and WGA have low affinity for the glycans of RNase B, these lectins were not expected to induce aggregation of the RNase B-modified gold nanoparticles. A buffer control

was also used to ensure that aggregation was not induced by changes in concentration; pH and ionic strength were maintained in all test solutions.

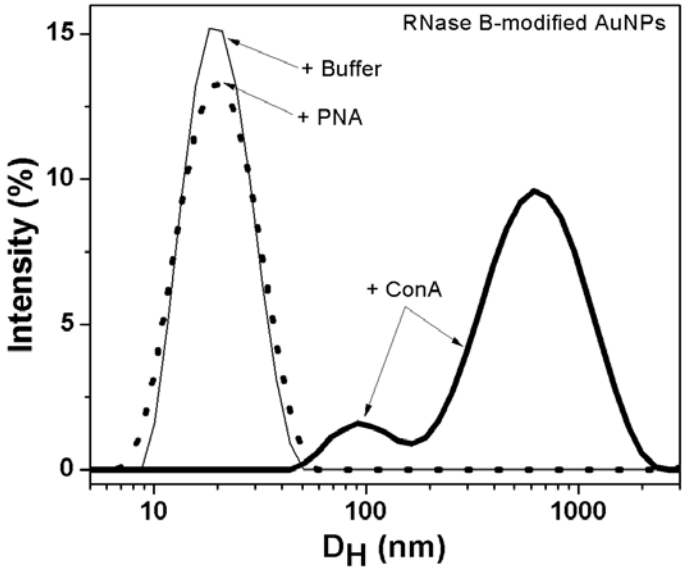


Figure 1. A plot of the intensity distribution of the hydrodynamic diameters, $D_H$, measured by dynamic light scattering, for RNase B-modified gold nanoparticles before (+ buffer) and after the addition of PNA (negative control) and Con A (binding) lectins.

The addition of a Con A solution to RNase B-modified gold nanoparticles resulted in changes to the nanoparticle size distribution as measured by DLS (Figure 1). The hydrodynamic diameter of the RNase B-modified gold nanoparticles increased on average from 21.3 nm ± 0.7 nm to a bimodal distribution with peaks observed at 90 nm ± 10 nm and 660 nm ± 50 nm approximately one minute after addition of Con A. These data are consistent with the proposed steps illustrated in Scheme I. The shift to a bimodal distribution of sizes has been reported in similar binding assays (Liu et al. 2008) and we attribute this behavior to a mixture of multimers of aggregated nanoparticles and larger aggregate species. No significant increase in the average hydrodynamic diameter was observed for the RNase B-modified gold nanoparticles upon addition of the non-binding PNA lectin (hydrodynamic diameter of 20 nm ± 1 nm, Figure 1).

Evidence for aggregation upon introduction of Con A to RNase B-modified gold nanoparticle samples was also seen in the UV-visible spectrum acquired approximately 1 minute after mixing (Figure 2). Specifically, the absorbance at all wavelengths increased and the plasmon shifted to the red by 4 nm, to 529 nm. These spectral changes were also discernable by eye as a decrease in transparency and a color change to red-purple. In contrast, addition of either of the non-mannose specific lectins, PNA or WGA, caused no change to the absorption spectrum.

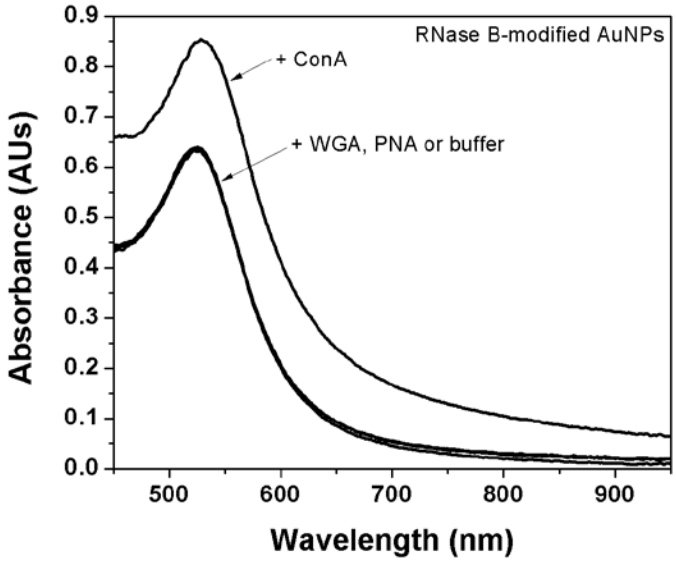


Figure 2. UV-visible spectra of RNase B-modified gold nanoparticles acquired approximately 1 min after the addition of Con A (binding lectin), WGA (negative control lectin), PNA (negative control lectin) or buffer. The final concentration of lectins in all cases was 50 μg/mL.

The red-shift of the plasmon band of the RNase-B modified gold nanoparticles after addition of Con A is due to increased interparticle plasmon coupling due to aggregation. As illustrated in Scheme 1, these aggregates likely consist of two or more gold nanoparticles, separated by a protein tri-layer (RNase B/Con A/RNase B). The distance between the RNase B/Con A/RNase B gold nanoparticle agglomerates can be estimated by the magnitude of the red-shift and the "plasmon ruler equation" (Jain et al. 2007) to be ≈ 7 nm. This distance corresponds well with a

reasonable estimate of the protein tri-layer thickness obtained by summing the thickness of the adsorbed RNase B protein layer (≈ 1.5 nm from DLS) and the reported size of a Con A tetramer (≈ 3 nm to ≈ 7.5 nm depending on orientation) (Shoham et al. 1979; Waner et al. 1998).

MALDI-TOF MS was used also used to confirm the presence of Con A in an aggregated sample of RNase B-modified gold nanoparticles exposed to Con A. After thorough rinsing to remove excess RNase B and Con A from the sample, peaks characteristic of Con A and RNase B were observed, providing further evidence that Con A is bound to the RNase-B modified gold nanoparticles. These results are provided in the Supplemental Information (Figures S-5 and S-6).

Visual evidence of Con A binding to the RNase B-modified Au NPs is observed with longer assay times. Larger aggregates, which sediment to the bottom of the vial and cause a decrease in the absorbance of the solution (Figure S-7), can be discerned by eye after 90 minutes of interaction. We found that faster results discernable by eye, not requiring instrumentation (e.g. a DLS or spectrophotomer), could be obtained by using mild centrifugation. Mild centrifugation (3000 r/min for 5 min) caused the aggregated particles to sediment to the bottom of a centrifuge tube, leaving a clear, colorless supernatant, observable by eye (Figure S-8, inset). In contrast, control mixtures using WGA and PNA, centrifuged identically were indistinguishable by eye to non-centrifuged suspensions of RNase B coated gold nanoparticles.

*Determination of Assay Specificity*

Two additional control experiments were performed to confirm that the optical changes observed for the RNase B-modified gold nanoparticles exposed to Con A are caused by specific lectin-oligosaccharide cross-linking of the particles. The first used inhibitory sugars to compete with lectin-glycan binding and the second used a non-glycosylated form of RNase B, RNase A.

Mannose and glucose are commonly used to elute glycoproteins purified from Con A agarose bead chromatographic columns. We expected that with the addition of an excess of these inhibitory sugars, the Con A sugar binding sites would be occupied and no change in the RNase B-modified gold nanoparticle suspension would be observed. The inhibitory sugar mixture of equal parts mannose and glucose was added to the Con A solution at a concentration of 500 mmol/L and incubated overnight. The Con A solution was then added to the RNase B modified-gold nanoparticles and the absorbance spectrum was measured after 1 min (Fig. 3a). This absorption spectrum was indistinguishable from the buffer-diluted RNase B-modified gold nanoparticles suggesting that the sugars effectively competed for binding with Con A versus the mannose-presenting groups of the RNase B-modified gold nanoparticle suspension. These data indicate that Con A binds specifically to the mannose-presenting groups and is responsible for aggregation of the RNase B-modified gold nanoparticles.

The amino acid sequence of RNase A is identical to RNase B; however, RNase A is non-glycosylated (Kuno et al. 2005). We prepared RNase A-modified gold nanoparticles following the same procedure for preparing RNase B-modified gold nanoparticles and repeated the UV-visible experiments. No discernable change in the UV-visible spectra was observed following addition of Con A or the other control species (PNA and WGA) to the RNase A-modified gold nanoparticles (Figure 3b) even after 150 minutes (Figure S-7d). Based on these experiments and the results described above, we conclude that the change in the measured nanoparticle plasmon absorbance and aggregation is mediated by specific lectin-oligosaccharide interactions between Con A and the mannose presenting groups of RNase B.

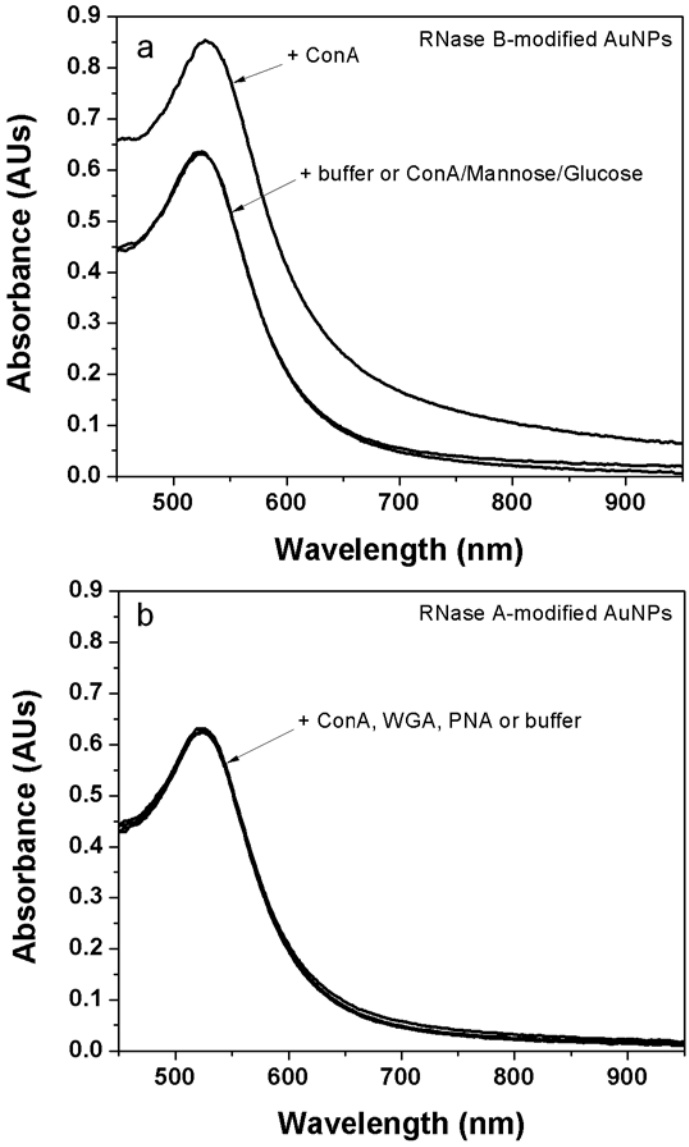


Figure 3**.** (a) UV-visible spectra of RNase B-modified gold nanoparticles approximately 1 min after the addition of Con A with (bottom trace) and without (top trace) the addition of an excess inhibitory sugar mixture of mannose and glucose which block binding of Con A. (b) Invariant UV-visible spectra of gold nanoparticles modified with RNase A (deglycosylated form of RNase B) approximately 1 min after the addition of Con A, WGA, PNA, or buffer.

*Determination of Assay Sensitivity*

To probe the sensitivity of the assay, the relative amount of RNase B adsorbed to each gold nanoparticle was controlled by varying the relative mole fraction of RNase B to RNase A during

the adsorption to the gold nanoparticles. During the glycoprotein adsorption step, the total glycoprotein solution concentration was maintained at 100 μg/mL and the molar composition of RNase B to RNase A was varied from 0 to 100%. Absorbance spectra for RNase B-modified gold nanoparticles at different mole ratios acquired approximately 1 minute after introduction of Con A are shown in Figure 4a. The $\lambda_{max}$ absorbance values increase with higher mol percent RNase B. A plot of the change in absorbance at $\lambda_{max}$ vs. mole % RNase B illustrates this trend (Figure 4b). A change in absorbance could be measured at solution concentrations of RNase B as low as 1 μg/mL (Figure 4a, 0% and 1% lines) after addition of Con A. This value is comparable to previously published limits of detection for similar systems (Thanh and Rosenzweig 2002). A linear response was observed for solution concentrations of RNase B below 5 μg/mL and no further change in absorbance was observed at concentrations above 20 μg/mL.

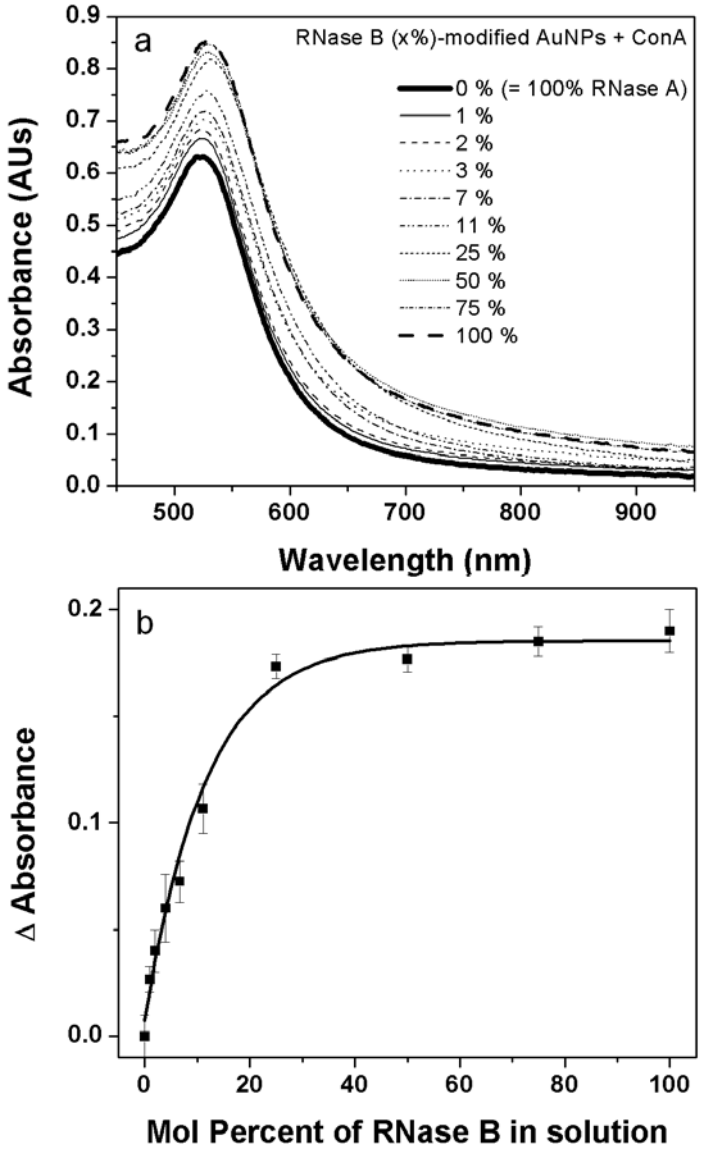


Figure 4**.** (a) UV-visible spectra of RNase B-modified gold nanoparticles approximately 1 min after the addition of Con A at various mole percent of RNase B. The relative amount of RNase B adsorbed to each gold nanoparticle was controlled by varying the relative mole fraction of RNase B to RNase A during the adsorption to the gold nanoparticles. The final concentration of Con A is 50 μg/mL. (b) Change in maximum absorbance measured at ≈ 529 nm for Con A as a function of RNase B solution mole percent. Error bars represent one standard deviation above and below the mean of at least 3 replicates.

*Characterization of rituximab-modified gold nanoparticles*

The assay was applied to a therapeutic monoclonal antibody, rituximab. Rituximab is an antibody of the IgG class and its glycans are covalently attached at asparagine 297 of each heavy

chain in the Fc region. The diantennary glycans of rituximab consist of a "core" heptasaccharide with additional *N*-acetylglucosamine (GlcNAc) and/or galactose moieties attached to the outer arms (Figure S-9). The oligosaccharides of rituximab constitute ≈ 2% of the mass of the ≈ 145 kDa protein. Therefore, the surface density of glycans for rituximab-modified gold nanoparticles is expected to be lower than that of the RNase B-modified gold nanoparticles.

Rituximab-Au NP conjugates were prepared by mixing rituximab and 30 nm Au NPs for one minute, followed by centrifugation, decanting of solution, and re-dispersion in water to remove excess rituximab. A minimum concentration of 0.1 mg/mL rituximab was required to stabilize the Au NPs, which was determined from salt-induced flocculation tests (Figure S-10). The adsorption of rituximab to Au NPs was confirmed by DLS, where the measured diameter increased from (26 $\pm$ 3) nm for the bare Au NPs to (58 $\pm$ 4) nm after conjugation with rituximab (Figure S-11). Uncertainties represent one standard deviation of at least three replicates. Rituximab-Au NP conjugate solutions prepared in this way exhibited a red-pink color (Figure S-12). Further evidence of rituximab adsorption was provided by the presence of protein amide I and amide II bands in the Fourier-transform infrared spectrum of rituximab modified Au NPs (Figure S-11).

*Glycoanalysis of rituximab by Gold Nanoparticles*

Lectin-induced aggregation of the rituximab-Au NP conjugates was monitored one minute after introduction of the lectins by DLS and UV-visible spectroscopy. WGA was examined as a potential binding lectin due to its affinity for GlcNAc residues. Both DLS and UV-visible measurements indicated binding and aggregation of the rituximab-modified Au NPs upon addition of WGA. Approximately one minute after addition of WGA, an increase in

hydrodynamic diameter of ≈ 13 nm was measured by DLS (Figure 5a), suggesting that binding of WGA to GlcNAc residues of the mAb results in aggregation of the mAb-Au NP conjugates. The addition of another lectin expected to bind to the glycans of rituximab, Con A, a mannose-binding lectin, also caused an increase in diameter (data not shown). Changes in the UV-visible spectra of the mAb Au NP conjugates after addition of WGA (Figure 5b) also suggested aggregation of the conjugates due to lectin-glycan binding. A reproducible increase in absorbance and red-shift of ≈ 4 nm was observed in the plasmon resonance band of the rituximab-Au NP conjugates one minute after addition of WGA, thus corroborating DLS results. We postulate that these optical shifts result from changes in the local refractive index around the Au NPs upon lectin binding to the oligosaccharides of the rituximab-Au NP conjugates or to scattering effects induced by the formation of aggregates. Furthermore, after 24 hours in the presence of WGA or Con A, solutions of the rituximab-Au NP conjugates turned from red pink to clear due to sedimentation of aggregates (Figure S-12).

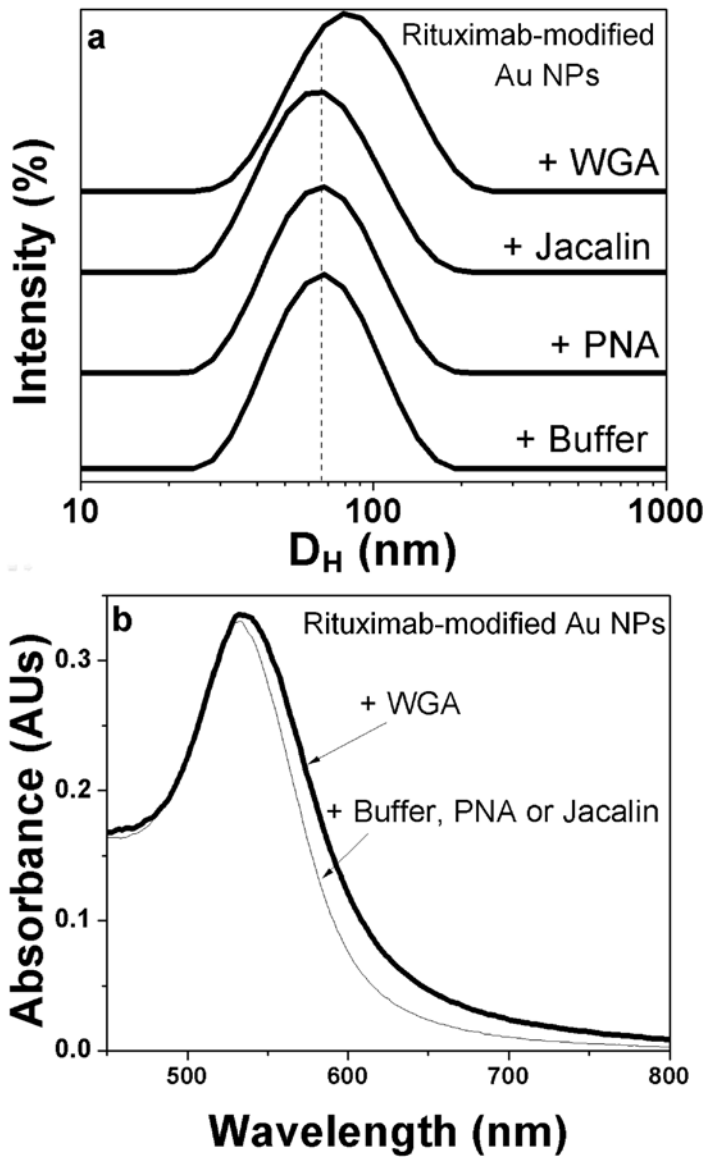


Figure 5. (a) DLS diameter results and (b) UV-visible spectra of rituximab-Au NP conjugates before (+ buffer) and approximately one minute after the addition of PNA (negative control), Jacalin (negative control), or WGA (binding lectin).

The effect of adding two negative control lectins was examined to verify that specific lectin-glycan interactions caused the observed aggregation. Jacalin (50 kDa) and PNA are multivalent lectins with high specificity for ß-D-Gal(1-3)-D-GalNAc residues and, thus should have low affinity for the glycans of rituximab. As expected, no significant increase in diameter was

observed using DLS after the addition of the non-binding control lectins, PNA or Jacalin, (Figure 5a). Similarly, no significant changes in the UV-visible spectra of the NPs were observed when PNA or Jacalin (Figure 5b) were added. Even after 24 hours in the presence of PNA or Jacalin, the rituximab-Au NP conjugates appeared stable as evidenced by their characteristic red-pink color (Figure S-12).

## CONCLUSIONS

We have demonstrated a rapid glycoanalysis method by lectin binding to RNase B- and rituximab-modified gold nanoparticles detected using either simple instrumentation (e.g. DLS or spectrophotometry) or by visual inspection. It is difficult to make a direct comparison of this method to LC and MS methods due to the wide range of instrumental protocols and sample preparation strategies that are used for glycan analysis. As is true for most gold nanoparticle aggregation-based assays, a significant advantage of the method presented here over more conventional glycoanalysis methods is its simplicity. It does not require release of the glycans from the glycoprotein, as is required for many LC and MS methods. In addition, the glycoprotein is conjugated to the Au NPs using simple non-specific adsorption, requires as little as 0.05 mg of glycoprotein (for rituximab) and no instrumentation, beyond a centrifuge, is required.

Finally, the total analysis time was approximately 20 min which includes conjugation of rituximab to the Au NPs (1 min); purification of the rituximab-Au NP conjugate by centrifugation (10 min); incubation with binding lectin (1 min); and detection by DLS or UV-visible (variable times dependent on acquisition conditions).

While this method could perhaps be used to interrogate unknown glycoproteins, it would likely find more utility as a qualitative, glycan differentiation method, using multiple binding lectins for assessing changes in the glycoprofile of well-characterized glycoproteins such as therapeutic proteins. For example, a different lectin solution could be contained in wells of a microtiter plate and small aliquots of the glycoprotein-Au NP conjugate could be added to each well. Because each lectin exhibits different selectivity depending on the oligosaccharide composition, different color or spectral changes may be detected in each well, providing a lectin binding fingerprint of the glycan.

The versatility of this method of glycoanalysis is potentially great due to the breadth of the assay design space which includes the class of glycoprotein analyzed, affinity molecule chosen, nanomaterial used, and solution conditions (e.g. pH, ionic strength) used for the assay. For example, the specificity of the assay may be improved or broadened by using different classes of affinity molecules, such as aptamers or antibodies with specific binding affinities towards carbohydrate sequences.

This type of assay is complementary to the detailed glycan characterization information obtained by more rigorous methods, such as chromatographic, mass spectrometric, and hybrid methods. This approach may prove useful for process development or process monitoring applications as a rapid, high-throughput method for detecting changes in glycan profiles of therapeutic glycoproteins.

ACKNOWLEDGEMENTS

Financial support was received by G.S.-P., T.A.M., and J.B.F. through the NRC-RAP/NIST postdoctoral fellowship program. The authors thank W.-L. Liao and I.V. Turko for the use of the

MALDI-TOF MS instrument and E. Eisenstein for the use of the AUC all located at the Institute for Bioscience and Biotechnology Research (IBBR), Rockville, MD. We also thank Kelly Ramsburg for her help with the flocculation tests.

REFERENCES

Blow N. 2009. Glycobiology: A spoonful of sugar. Nature 457(7229):617-622.

Brewer SH, Glomm WR, Johnson MC, Knag MK, Franzen S. 2005. Probing BSA binding to citrate-coated gold nanoparticles and surfaces. Langmuir 21(20):9303-9307.

Brooks SA. 2009. Strategies for Analysis of the Glycosylation of Proteins: Current Status and Future Perspectives. Mol Biotechnol 43(1):76-88.

Chen S, Zheng T, Shortreed MR, Alexander C, Smith LM. 2007. Analysis of Cell Surface Carbohydrate Expression Patterns in Normal and Tumorigenic Human Breast Cell Lines Using Lectin Arrays. Anal Chem 79:5698-5702.

Chirino AJ, Mire-Sluis A. 2004. Characterizing biological products and assessing comparability following manufacturing changes. Nature Biotech 22(11):1383-1391.

Cho K, Lee Y, Lee C-H, Lee K, Kim Y, Choi H, Ryu P-D, Lee SY, Joo S-W. 2008. Selective Aggregation Mechanism of Unmodified Gold Nanoparticles in Detection of Single Nucleotide Polymorphism. J Phys Chem C 112:8629-8633.

Cunningham S, Gerlach JQ, Kane M, Joshi L. 2010. Glyco-biosensors: Recent advances and applications for the detection of free and bound carbohydrates. Analyst 135(10):2471-2480.

Dai Z, Kawde AN, Xiang Y, La Belle JT, Gerlach J, Bhavanandan VP, Joshi L, Wang J. 2006. Nanoparticle-based sensing of glycan-lectin interactions. J Am Chem Soc 128(31):10018-10019.

Dasary SSR, Senapati D, Singh AK, Anjaneyulu Y, Yu HT, Ray PC. 2010 Highly Sensitive and Selective Dynamic Light-Scattering Assay for TNT Detection Using p-ATP Attached Gold Nanoparticle. ACS Applied Materials & Interfaces 2(12):3455-3460.

Dell A, Morris HR. 2001. Glycoprotein Structure Determination by Mass Spectrometry. Science 291:2351-2356.

Elghanian R, Storhoff JJ, Mucic RC, Letsinger RL, Mirkin CA. 1997. Selective colorimetric detection of polynucleotides based on the distance-dependent optical properties of gold nanoparticles. Science 277(5329):1078-1081.

Fromell K, Andersson M, Elihn K, Caldwell KD. 2005. Nanoparticle decorated surfaces with potential use in glycosylation analysis. Colloids Surf, B 46(2):84-91.

Fu D, Chen L, O'Neill RA. 1994. A detailed structural characterization of ribonuclease B oligosaccharides by 1H NMR spectroscopy and mass spectrometry. Carbohydr Res 261:173-186.

Gao JQ, Liu DJ, Wang ZX. 2008. Microarray-Based Study of Carbohydrate-Protein Binding by Gold Nanoparticle Probes. Anal Chem 80(22):8822-8827.

Hirabayashi J. 2008. Concept, Strategy, and Realization of Lectin-based Glycan Profiling. J Biochem 144:139-147.

Hwang GM, Pang L, Mullen EH, Fainman Y. 2008. Plasmonic Sensing of Biological Analytes Through Nanoholes. IEEE Sens J 8(11-12):2074-2079.

Jain PK, Huang WY, El-Sayed MA. 2007. On the universal scaling behavior of the distance decay of plasmon coupling in metal nanoparticle pairs: A plasmon ruler equation. Nano Lett 7(7):2080-2088.

Jans H, Liu X, Austin L, Maes G, Huo Q. 2009. Dynamic Light Scattering as a Powerful Tool for Gold Nanoparticle Bioconjugation and Biomolecular Binding Studies. Anal Chem 81(22):9425-9432.

Jefferis R. 2005. Glycosylation of Recombinant Antibody Therapeutics. Biotechnol Prog 21:11-16.

Kamoda S, Kakehi K. 2006. Capillary electrophoresis for the analysis of glycoprotein pharmaceuticals. Electrophoresis 27:2495-2504.

Kaur J, Singh KV, Boro R, Thampi KR, Raje M, Varshney GC, Suri CR. 2007. Immunochromatographic Dipstick Assay Format Using Gold Nanoparticles Labeled Protein-Hapten Conjugate for the Detection of Atrazine. Environ Sci Technol 41:5028-5036.

Kawasaki N, Ohta M, Hyuga S, Hashimoto O, Hayakawa T. 1999. Analysis of Carbohydrate Heterogeneity in a Glycoprotein Using Liquid Chromatography/Mass Spectrometry and Liquid Chromatography with Tandem Mass Spectrometry. Anal Biochem 269(2):297-303.

Kim YP, Park S, Oh E, Oh YH, Kim HS. 2009. On-chip detection of protein glycosylation based on energy transfer between nanoparticles. Biosens Bioelectron 24(5):1189-1194.

Kuno A, Uchiyama N, Koseki-Kuno S, Ebe Y, Takashima S, Yamada M, Hirabayashi J. 2005. Evanescent-field fluorescence-assisted lectin microarray: a new strategy for glycan profiling. Nature Methods 2(11):851-856.

Lacerda SHD, Park JJ, Meuse C, Pristinski D, Becker ML, Karim A, Douglas JF. 2009. Interaction of Gold Nanoparticles with Common Human Blood Proteins. ACS Nano 4(1):365-379.

Liang CH, Wang CC, Lin YC, Chen CH, Wong CH, Wu CY. 2009. Iron Oxide/Gold Core/Shell Nanoparticles for Ultrasensitive Detection of Carbohydrate-Protein Interactions. Anal Chem 81(18):7750-7756.

Lim A, Reed-Bogan A, Harmon BJ. 2008. Glycosylation profiling of a therapeutic recombinant monoclonal antibody with two N-linked glycosylation sites using liquid chromatography coupled to a hybrid quadrupole time-of-flight mass spectrometer. Anal Biochem 375:163-172.

Liu J, Lu Y. 2004. Accelerated Color Change of Gold Nanoparticles Assembled by DNAzymes for Simple and Fast Colorimetric Pb2+ Detection. J Am Chem Soc 126:12298-12305.

Liu X, Dai Q, Austin L, Coutts J, Knowles G, Zou JH, Chen H, Huo Q. 2008. A one-step homogeneous immunoassay for cancer biomarker detection using gold nanoparticle probes coupled with dynamic light scattering. J Am Chem Soc 130(9):2780-2782.

Liu Y, Mernaugh RL, Zeng XQ. 2009. Single chain fragment variable recombinant antibody functionalized gold nanoparticles for a highly sensitive colorimetric immunoassay. Biosens Bioelectron 24(9):2853-2857.

Liz-Marzán LM. 2006. Tailoring Surface Plasmons through the Morphology and Assembly of Metal Nanoparticles. Langmuir 22:32-41.
Loris R, Hamelryck T, Bouckaert J, Wyns L. 1998. Legume lectin structure. Biochim Biophys Acta 1383:9-36.
Medley CD, Smith JE, Tang Z, Wu Y, Bamrungsap S, Tan W. 2008. Gold Nanoparticle-Based Colorimetric Assay for the Direct Detection of Cancerous Cells. Anal Chem 80:1067-1072.
Morris T, Copeland H, McLinden E, Wilson S, Szulczewski G. 2002. The Effects of Mercury Adsorption on the Optical Response of Size-Selected Gold and Silver Nanoparticles. Langmuir 18(20):7261-7264.
Mulvaney P. 1996. Surface plasmon spectroscopy of nanosized metal particles. Langmuir 12(3):788-800.
Nam JM, Thaxton CS, Mirkin CA. 2003. Nanoparticle-based bio-bar codes for the ultrasensitive detection of proteins. Science 301(5641):1884-1886.
Obare SO, Hollowell RE, Murphy CJ. 2002. Sensing Strategy for Lithium Ion Based on Gold Nanoparticles. Langmuir 18:10407-10410.
Rini JM. 1995. Lectin Structure. Annu Rev Biophys Biomol Struct 24:551-577.
Rudd PM, Elliott T, Cresswell P, Wilson IA, Dwek RA. 2001. Glycosylation and the immune system. Science 291(5512):2370-2376.
Rudd PM, Joao HC, Coghill E, Fiten P, Saunders MR, Opdenakker G, Dwek RA. 1994. Glycoforms modify the dynamic stability and functional-activity of an enzyme. Biochemistry 33(1):17-22.
Sardar R, Funston AM, Mulvaney P, Murray RW. 2009. Gold Nanoparticles: Past, Present, and Future. Langmuir 25(24):13840-13851.
Schneider CK. 2008. Monoclonal Antibodies - Regulatory Challenges. Curr Pharm Biotechnol 9(6):431-438.
Schofield CL, Field RA, Russell DA. 2007. Glyconanoparticles for the Colorimetric Detection of Cholera Toxin. Anal Chem 79:1356-1361.
Schofield CL, Haines AH, Field RA, Russell DA. 2006. Silver and Gold Glyconanoparticles for Colorimetric Bioassays. Langmuir 22:6707-6711.
Shoham M, Yonath A, Sussman JL, Moult J, Traub W, Kalbgilboa AJ. 1979. Crystal-Structure of Demetallized Concanavalin-a - Metal-Binding Region. J Mol Biol 131(2):137-155.
Si S, Kotal A, Mandal TK. 2007. One-Dimensional Assembly of Peptide-Functionalized Gold Nanoparticles: An Approach Toward Mercury Ion Sensing. J Phys Chem C 111:1248-1255.
Sparbier K, Koch S, Kessler I, Wenzel T, Kostrzewa M. 2005. Selective Isolation of Glycoproteins and Glycopeptides for MALDI-TOF MS Detection Supported by Magnetic Particles. J Biomol Techniques 16(4):407-413.
Storhoff JJ, Elghanian R, Mucie RC, Mirkin CA, Letsinger RL. 1998. One-Pot Colorimetric Differentiation of Polynucleotides with Single Base Imperfections Using Gold Nanoparticle Probes. J Am Chem Soc 120:1959-1964.
Tarelli E, Byers HL, Wilson M, Roberts G, Homer KA, Beighton D. 2000. Dettecting Mannoside Activities Using Ribonuclease B and Matrix-Assisted Laser Desorption/Ionization-Time of Flight Mass Spectrometry. Anal Biochem 282:165-172.

Tessier PM, Jinkoji J, Cheng YC, Prentice JL, Lenhoff AM. 2008. Self-interaction nanoparticle spectroscopy: A nanoparticle-based protein interaction assay. J Am Chem Soc 130(10):3106-3112.

Thanh NTK, Rosenzweig Z. 2002. Development of an Aggregation-Based Immunoassay for Anti-Protein A Using Gold Nanoparticles. Anal Chem 74:1624-1628.

Thobhani S, Attree S, Boyd R, Kumarswami N, Noble J, Szymanski M, Porter RA. 2010 Bioconjugation and characterisation of gold colloid-labelled proteins. J Immunol Methods 356(1-2):60-9.

Thomas GB, Rader LH, Park J, Abezgauz L, Danino D, DeShong P, English DS. 2009. Carbohydrate Modified Catanionic Vesicles: Probing Multivalent Binding at the Bilayer Interface. Journal of the American Chemical Society 131(15):5471-5477.

Toyoshima M, Miura Y. 2009. Preparation of Glycopolymer-Substituted Gold Nanoparticles and Their Molecular Recognition. J Polym Sci, Part A: Polym Chem 47:1412-1421.

van Kooyk Y, Rabinovich GA. 2008. Protein-glycan interactions in the control of innate and adaptive immune responses. Nature Immunol 9(6):593-601.

Walsh G, Jefferis R. 2006. Post-translational modifications in the context of therapeutic proteins. Nature Biotech 24(10):1241-1252.

Waner MJ, Gilchrist M, Schindler M, Dantus M. 1998. Imaging the molecular dimensions and oligomerization of proteins at liquid/solid interfaces. J Phys Chem B 102(9):1649-1657.

Wang X, Ramstrom O, Yan MD. 2010. Quantitative Analysis of Multivalent Ligand Presentation on Gold Glyconanoparticles and the Impact on Lectin Binding. Anal Chem 82(21):9082-9089.

Watanabe S, Yoshida K, Shinkawa K, Kumagawa D, Seguchi H. 2010. Thioglucose-stabilized gold nanoparticles as a novel platform for colorimetric bioassay based on nanoparticle aggregation. Colloids Surf, B 81(2):570-577.

Yang XH, Huang JH, Wang Q, Wang KM, Yang LJ, Huo XQ. 2011. A one-step sensitive dynamic light scattering method for adenosine detection using split aptamer fragments. Analytical Methods 3(1):59-61.

Zamfir A, Peter-Katalinic J. 2004. Capillary electrophoresis-mass spectrometry for glycoscreening in biomedical research. Electrophoresis 25(13):1949-1963.

Zand R, Agrawal BBL, Goldstei.Ij. 1971. pH-dependent conformational changes of concanavalin-A. Proc Natl Acad Sci U S A 68(9):2173-2176.

Zhang J, Du J, Yan M, Dhaliwal A, Wen J, Liu F, Segura T, Lu Y. 2011. Synthesis of protein nano-conjugates for cancer therapy. Nano Research 4(5):425-433.

# A Lectin-Based Gold Nanoparticle Assay for Probing Glycosylation of Glycoproteins

*Germarie Sánchez-Pomales, Todd A. Morris, James B. Falabella, Michael J. Tarlov and*

*Rebecca A. Zangmeister**

Bioprocess Measurements Group, Biochemical Science Division, National Institute of Standards and Technology, 100 Bureau Dr., MS 8362, Gaithersburg, MD 20899-8362

*rebecca.zangmeister@nist.gov; telephone: 301-975-4912; fax: 301-975-2643

Supplementary Material Table of Contents

I. Methodology: Instrumentation

*X-ray photoelectron spectroscopy (XPS) analyses*

X-ray photoelectron spectroscopy (XPS) was performed on a Kratos Axis Ultra$^{DLD}$ instrument with monochromatic Al Kα radiation (1486.7 eV). Survey scans were obtained for unmodified and RNase B-modified gold nanoparticles in the fixed analyzer transmission mode with pass energy of 160 eV. The binding energies were calibrated with respect to the gold 4f 7/2 peak at 84.0 eV. We prepared the XPS samples by first washing away salts and excess protein from the gold colloids by repeatedly centrifuging the samples at 13200 r/min for 40 min, discarding the supernatant, adding water, and mixing by vortex to suspend the colloids. This process was repeated at least twice. A small aliquot (10 μL to 15 μL) of the concentrated colloid was then drop cast and allowed to dry on a clean piece of indium foil for analysis. We determined the number of wash steps necessary by monitoring the Na 1s signal at ≈1070 eV. For insufficiently washed samples, sodium from NaOH added for pH control was detected by XPS.

*Analytical ultracentrifugation analyses*

Analytical ultracentrifugation (AUC) data were acquired with a Beckman XL-A analytical ultracentrifuge using a 4 place titanium rotor (model An-60 Ti). Sample cells were outfitted with 12 mm path length dual sector Epon™ centerpieces. The reference cell was filled with 425 μL of water and the sample cell was filled with 400 μL of either unmodified or RNase B-modified gold nanoparticles. We washed the RNase B-modified gold particles to remove excess salts and protein as was done with the samples for XPS analysis. Run conditions of the AUC for all samples were set as follows: temperature of 20 °C; absorbance wavelength of 520

nm (to correspond with the maximum in the absorbance spectrum of the gold particles); scan step size of 0.007 cm; rotation speed of 10000 r/min; and absorbance scan rate of once every 2 min. The raw centrifugation data was converted into sedimentation coefficient distributions using a continuous c(s) distribution model in Sedfit (Schuck 2000).

*MALDI-TOF Mass Spectral analyses*

Matrix-assisted laser desorption-ionization time-of-flight mass spectrometry (MALDI-TOF MS) data were collected with an Applied Biosystems instrument in the positive ion and linear modes using a 337 nm nitrogen laser for irradiating samples. Ions generated from 6000 laser pulses were collected and averaged for each spectrum. The matrix solution for all MALDI experiments was prepared by dissolving sinapinic acid (Fisher) at a concentration of 20 mg/mL in a solution of trifluoroacetic acid / acetonitrile / water (0.1:50:50 v/v/v). The sample was mixed with an equal volume of matrix solution. A 0.5 μL aliquot of the resulting solution was spotted onto a MALDI target plate and allowed to air dry prior to analysis.

*Fourier transform infrared spectroscopy (FT-IR)*

Fourier transform infrared spectroscopy (FT-IR) spectra were recorded on a Bio-Rad FTS 7000 series spectrometer. At least 512 scans were collected with a resolution of 2 $cm^{-1}$ for each sample. Samples were prepared by depositing 50 μL of the desired sample on a Teflon IR card (Sigma-Aldrich) and left to dry in a laminar flow hood prior to FT-IR measurements.

II. Dynamic Light Scattering

DLS results further confirmed the adsorption of RNase B to gold nanoparticles. The measured hydrodynamic diameter of the gold nanoparticles increased from 17.9 nm ± 0.5 nm for the bare gold nanoparticles to 21.3 nm ± 0.7 nm after conjugation with RNase B (Figure S-4).

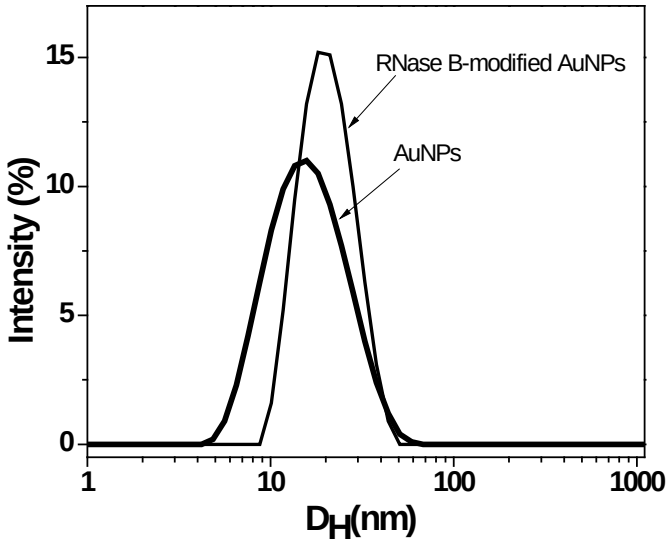


Figure S-1 Dynamic light scattering results showing an increase in hydrodynamic size for the bare gold nanoparticles after conjugation with RNase B.

III. XPS Characterization of modified gold nanoparticles

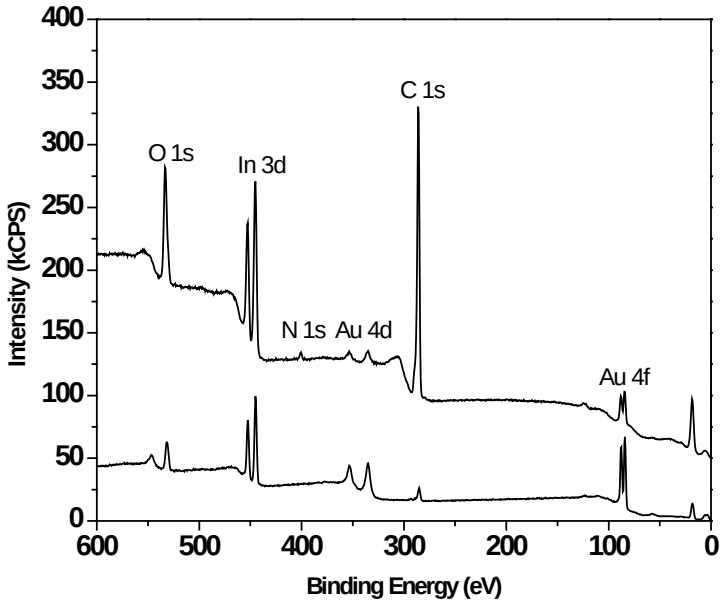


Figure S-2**.** XPS survey scan of an aliquot of washed gold nanoparticles (bottom spectrum) and RNase B-modified gold nanoparticles (top spectrum) dried on indium foil.

X-ray photoelectron spectroscopy (XPS) was used as a qualitative indicator that adsorption of the glycoprotein to the nanoparticles had occurred. Figure S-2 is a survey spectrum of an aliquot of washed RNase B-modified gold nanoparticles on a piece of indium foil. Present in the spectrum are XPS peaks due to indium (In 3d at ≈445 eV), carbon (C 1s at ≈285 eV), oxygen (O 1s at ≈533 eV), nitrogen (N 1s at ≈401 eV), and gold (Au 4f at ≈84 eV). We expected the presence of carbon, oxygen, nitrogen, and gold from the RNase B-modified gold nanoparticles. Although the composition of RNase B includes carbon and oxygen and these elements could serve as indicators of protein adsorption to the nanoparticle surface, their presence could also be attributed to citrate ions (of the citrate-stabilized colloids) (Brewer et al. 2005; Tsai et al. 2008) and adventitious hydrocarbon contamination. However, in the current study, the nitrogen XPS

signal is unique to the protein-modified nanoparticles and demonstrates that RNase B is adsorbed to the surface of the gold nanoparticle.

IV. AUC characterization of modified gold nanoparticles

Analytical ultracentrifugation (AUC) of both unmodified and RNase B-modified gold nanoparticle samples was performed. In AUC, the sample is centrifuged and the extent of sedimentation through the sample cell is monitored by periodically measuring the absorbance of the sample along the length of the sample cell. We performed AUC sedimentation experiments for both bare 10 nm gold particles and nanoparticles modified with RNase B. The sedimentation coefficient, as shown in equation 1, is defined as the terminal velocity of the particle over the strength of the instantaneous gravitational field in the centrifuge,

$$s = v_t / \vec{g} \qquad \text{(S-E1)}$$

where $s$ is the sedimentation coefficient of the particle, $v_t$ is the particle's terminal velocity, and $\vec{g}$ is the instantaneous gravitational field in the centrifuge. The sedimentation coefficient is often reported in units of Svedbergs (S). One Svedberg is equal to $10^{-13}$ seconds. The particle mass and density and the viscosity of the matrix fluid can affect the terminal velocity of the particle. The Svedberg equation is derived from a force balance between the centripetal force, friction force, and buoyant force and illustrates that as particle density decreases, the sedimentation coefficient decreases,

$$s = \frac{DM\left(1 - \bar{v}\rho_f\right)}{RT} \qquad \text{(S-E2)}$$

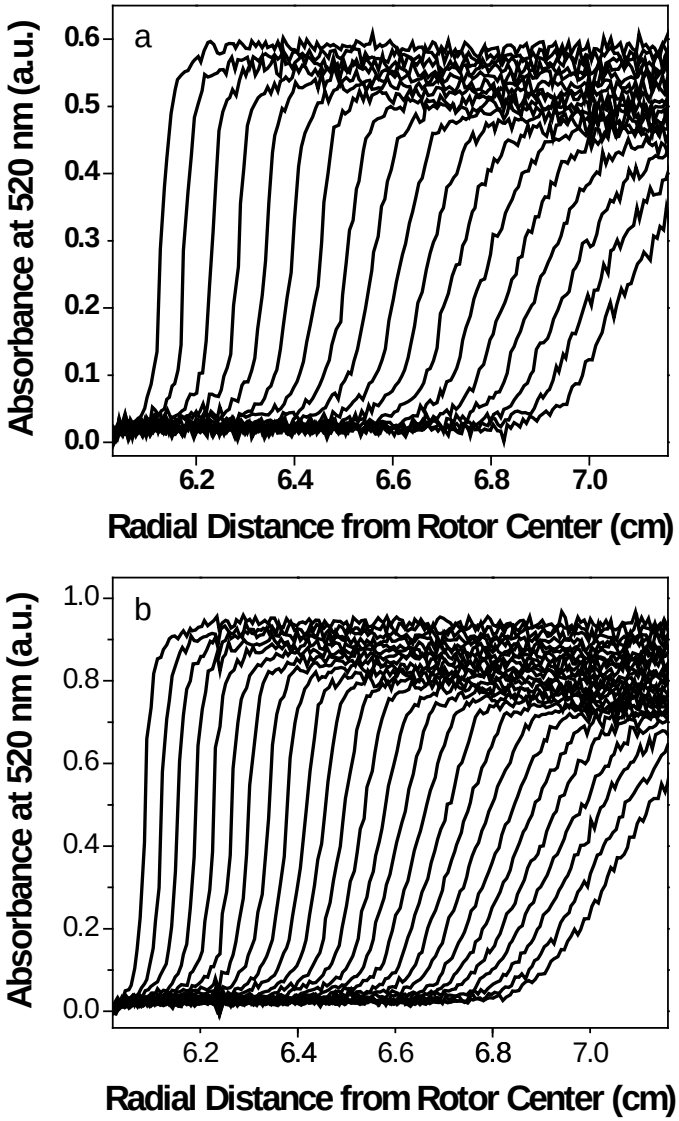


Figure S-3. Raw AUC UV/Vis absorbance data obtained from scans of (a) bare 10 nm gold particles and (b) RNase B coated 10 nm gold particles both at pH 10. Both samples were sedimented at 10000 r/min and scans were taken every 2 min.

where s is the sedimentation coefficient of the particles, $D$ is the diffusion coefficient of the suspended particle, $M$ is the mass of the sedimenting particle, $\bar{\nu}$ is the partial specific volume of the sedimenting particle, $\rho_f$ is the density of the matrix fluid, $R$ is the gas constant, and $T$ is the sample temperature (in kelvins). From the sedimentation coefficient we qualitatively infer

particle characteristics before and after modification with the glycoprotein. Figure S-3 shows the AUC absorbance scans at a wavelength of 520 nm of bare 10 nm and RNase B-modified 10 nm gold nanoparticles. Each consecutive trace (left-to-right) is a measure of the sedimentation front of the particles at two minute intervals. The spacing between consecutive scans is an indicator of the sedimentation rate of the particles. As shown in this figure, consecutive scans of RNase B-coated gold nanoparticles have a narrower spacing than for the bare gold nanoparticles. Because of this difference, we conclude that the RNase B-coated gold nanoparticles sediment more slowly than the bare gold nanoparticles. We determined the sedimentation coefficient distributions with the program Sedfit by numerically fitting the Lamm equation to the absorbance scans in Figure S-3 (Schuck 2000). Figure S-4 plots the sedimentation coefficient distributions of bare gold nanoparticles and for RNase B-modified nanoparticles. As shown in Figure S-4, the sedimentation coefficient of the RNase B-modified gold nanoparticles (≈490 S) is lower than the sedimentation coefficient of the bare nanoparticles (≈650 S). We expect that adsorption of RNase B will reduce the overall density of the nanoparticles, increasing the buoyancy of the particle. According to equation 2, a higher $\bar{\nu}$ (inversely proportional to particle density) will shift the sedimentation coefficient distribution to lower values.

These results are consistent with another AUC study of protein-conjugated gold nanoparticles in which gold nanoparticles were conjugated with lac repressor protein (lacI) and, in good agreement with theoretical predictions, were reported to have a lower sedimentation coefficient distribution than the bare nanoparticles (Calabretta et al. 2005).

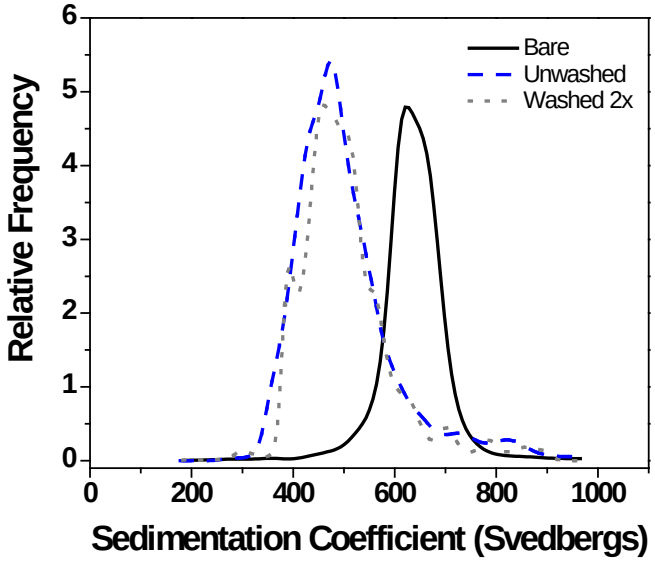


Figure S-4. Sedimentation coefficient distributions for bare 10 nm gold particles and 10 nm gold particles modified with RNase B.

The sedimentation coefficient distribution of the bare gold nanoparticles is asymmetric which may be attributable to polydispersity in nanoparticle diameters. In Figure S-4, we observe a shift to lower sedimentation coefficient values after addition of RNase B. Furthermore, to determine the optimal concentration for glycoprotein adsorption, the sedimentation coefficient was determined for stock concentrations of RNase B varying from 0.25 mg/mL to 2 mg/mL at a constant concentration of gold nanoparticles. The sedimentation coefficient decreased with increasing stock RNase B concentration until reaching a minimum value at 1.0 mg/mL. The sedimentation coefficient distribution remained constant at stock RNase B concentrations above 1.0 mg/mL, indicating that the maximum surface coverage of RNase B was attained at that stock concentration. Because the RNase B stock solution is mixed in a 1:10 v/v ratio with the gold nanoparticle solution, the final RNase B concentration is 0.1 mg/mL when mixed with the

nanoparticles. Finally, multiple washing of RNase B-modified particles with buffer resulted in little change to the AUC determined sedimentation coefficient suggesting largely irreversible adsorption of RNase B to the gold nanoparticle surface.

V. MALDI-TOF MS analysis of Con A bound to RNase B-modified gold nanoparticles

To further corroborate lectin binding to the RNase B-modified nanoparticles, MALDI-TOF MS was used to confirm the presence of Con A and RNase B in a sample of aggregated RNase B-modified gold nanoparticles that had been exposed to Con A overnight. Care was taken to ensure that there was no excess Con A or RNase B present in the sample as described below. Figure S-5 shows a representative MALDI-TOF MS spectrum.

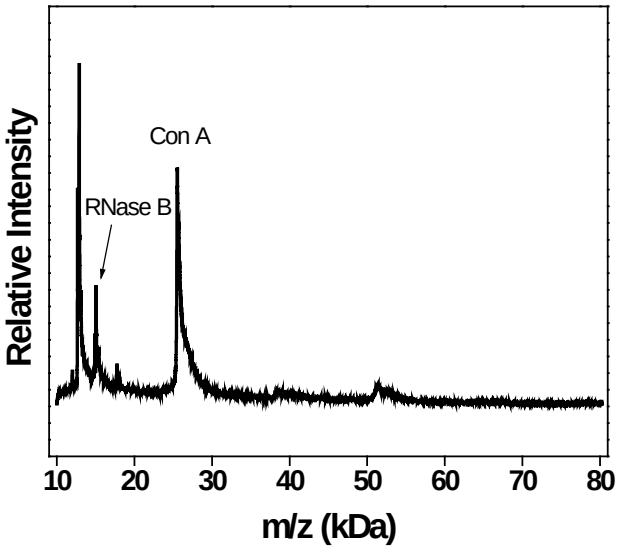


Figure S-5. MALDI TOF mass spectra of RNase B-modified gold nanoparticles after exposure to Con A and thorough rinsing to remove excess RNase B and Con A.

As expected, the spectrum displays peaks characteristic of Con A and RNase B. The peak centered near m/z ≈25 550 is assigned to the [M+H]+ monomer of Con A, and the peaks between ≈14 900 and 15 550 are assigned to [M+H]+ pseudo-ions of the various RNase B glycoforms. The MALDI-TOF mass spectrum of the washed nanoparticles provides further evidence to suggest that Con A is specifically bound to the RNase B-modified gold nanoparticles through lectin-oligosaccharide interactions.

To qualitatively measure washing efficiency, bovine serum albumin (BSA) was used as a protein marker and added to the Con A / RNase B-modified gold flocculated nanoparticles at a concentration equal to the concentration of Con A. We chose BSA as a marker for several reasons. First, as neither a glycoprotein nor a lectin, it was not expected to interfere with the RNase B-Con A interaction. Second, its most abundant MALDI ions (i.e., $[M+H]^+$ and $[M+2H]^+$ at approximate m/z values of 66,840 and 33,420, respectively) do not interfere with those of Con A or RNase B. After mixing BSA with the flocculated particles, the sample was centrifuged for 40 min at 13,200 r/min. The supernatant was collected and saved for analysis, while the precipitates were dispersed in fresh HBS buffer and centrifuged again for 40 min at 13200 r/min. HBS buffer was used for the washing steps to ensure that Con A did not lose its ability to bind to the RNase B-modified gold nanoparticles. We repeated this process of washing/centrifuging/supernatant removal three times. After the final centrifuge step, both the supernatant and washed flocculated nanoparticles were collected for MALDI-TOF MS analysis. We analyzed the supernatant to ascertain if washing was thorough enough to remove any loosely bound protein. If the washing steps were incomplete, this last supernatant was expected to contain residual Con A and BSA. Figure S-6 shows representative MALDI-TOF MS results for these three samples, where the spectra are offset for clarity.

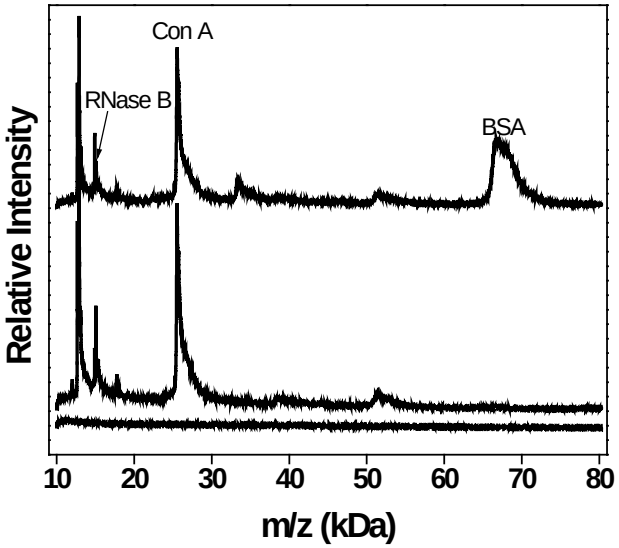


Figure S-6: MALDI TOF mass spectra of RNase B-modified gold nanoparticles after introduction of Con A and BSA. The top trace is the spectrum of the supernatant from the first centrifugation. The middle trace is the spectrum of the washed particles. The bottom trace is the spectrum of the supernatant from the last centrifugation. The spectra have been offset and scaled for clarity.

The top trace of Figure S-6 is the MALDI-TOF MS of the supernatant from the first wash step. As expected, this spectrum displays peaks characteristic of Con A, BSA, and RNase B. The peak centered near m/z ≈66 840 is assigned to the $[M+H]^+$ of BSA, that near m/z ≈25 550 is assigned to the $[M+H]^+$ monomer of Con A, and the peaks between ≈14 900 and ≈15 550 are assigned to $[M+H]^+$ pseudo-ions of the various RNase B glycoforms. The bottom spectrum is the MALDI-TOF MS of the supernatant from the final wash step. After repeated washings, RNase B, Con A, and BSA in the supernatant are undetectable indicating that the washing procedure is

sufficient to remove proteins that are loosely bound to nanoparticles. The middle spectrum is the MALDI-TOF MS of the nanoparticles as discussed above (Figure S-5).

VI. Additional UV-Visible Spectra

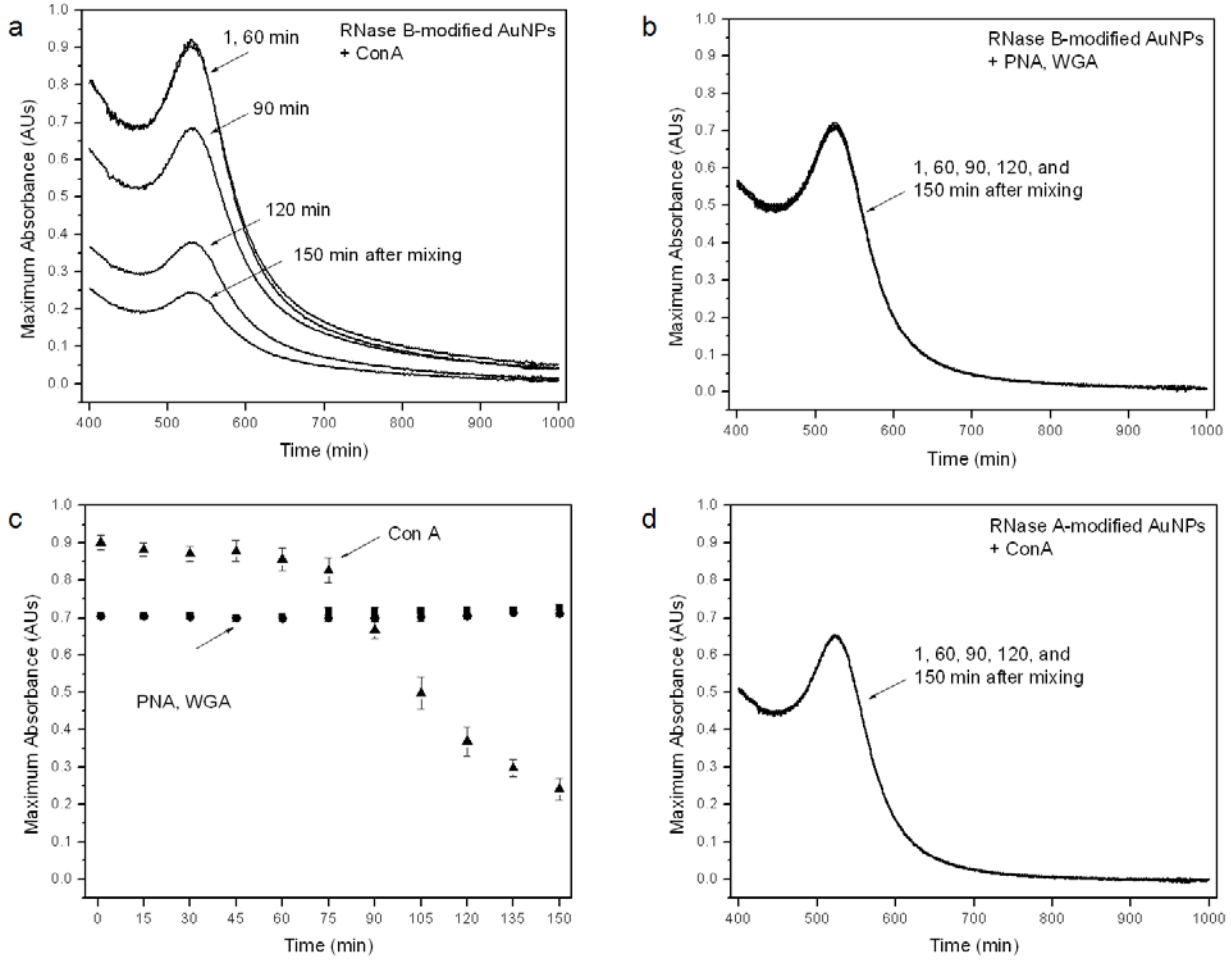


Figure S-7 (a) UV-Vis spectra of RNase B-modified gold nanoparticles 1, 60, 90, 120, and 150 min after introduction of Con A. (b) UV-Vis spectra of RNase B-modified gold nanoparticles 1 min, 60 min, 90 min, 120 min, and 150 min after introduction of PNA or WGA. (c) Change in maximum absorbance (absorbance at surface plasmon wavelength) with time for RNase B-modified gold nanoparticles after exposure to Con A(●), WGA(▲), or PNA (□). Error bars

represent one standard deviation above and below the mean of at least 3 replicates. (d) UV-Vis spectra of RNase A-modified gold nanoparticles 1, 60, 90, 120, and 150 min after introduction of Con A.

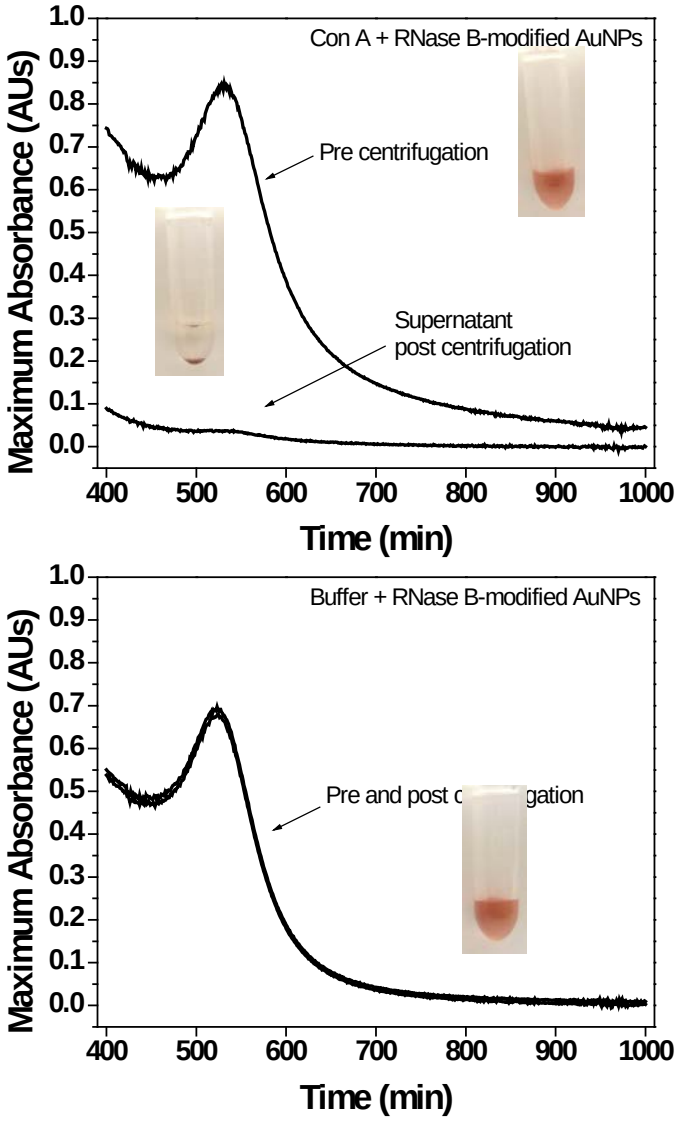


Figure S-8 (top) UV-Vis spectra of RNase B-modified gold nanoparticles after introduction of Con A and the sample supernatant after centrifugation at 3,000 r/min for 5 min. (bottom) UV-Vis spectra of RNase B-modified gold nanoparticles before and after centrifugation at 3000 r/min for 5 min.

VII. Structures of the main glycoforms of rituximab

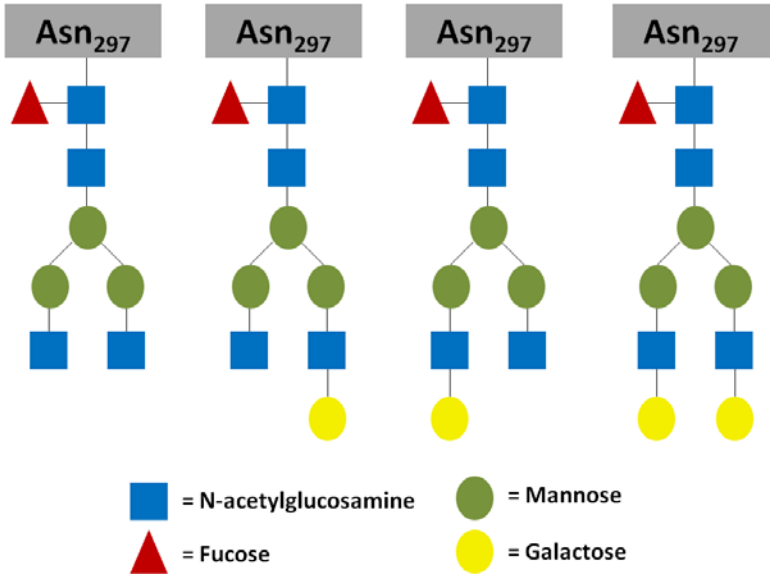


Figure S-9. Main N-linked glycoforms of rituximab

VIII. Flocculation Tests

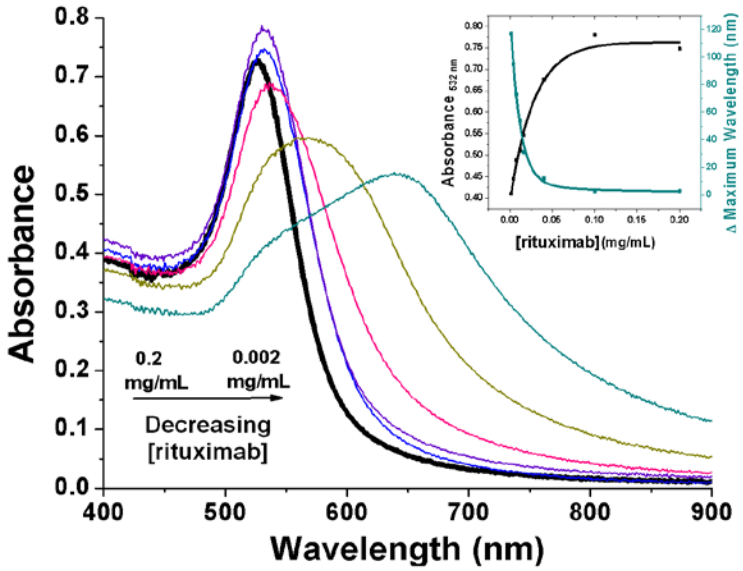


Figure S-10. Flocculation test results: UV-visible spectra after the addition of 10% NaCl by mass to rituximab-Au NP conjugates prepared with rituximab concentrations ranging from 0.002 mg/mL to 0.2 mg/mL; UV-visible spectrum of the bare Au NPs before addition of NaCl (black) is shown for comparison. Inset: Graph showing changes in the wavelength of maximum absorbance, as well as the absorbance at 532 nm as a function of rituximab concentration.

IX. Evidence of rituximab conjugation to Au NPs

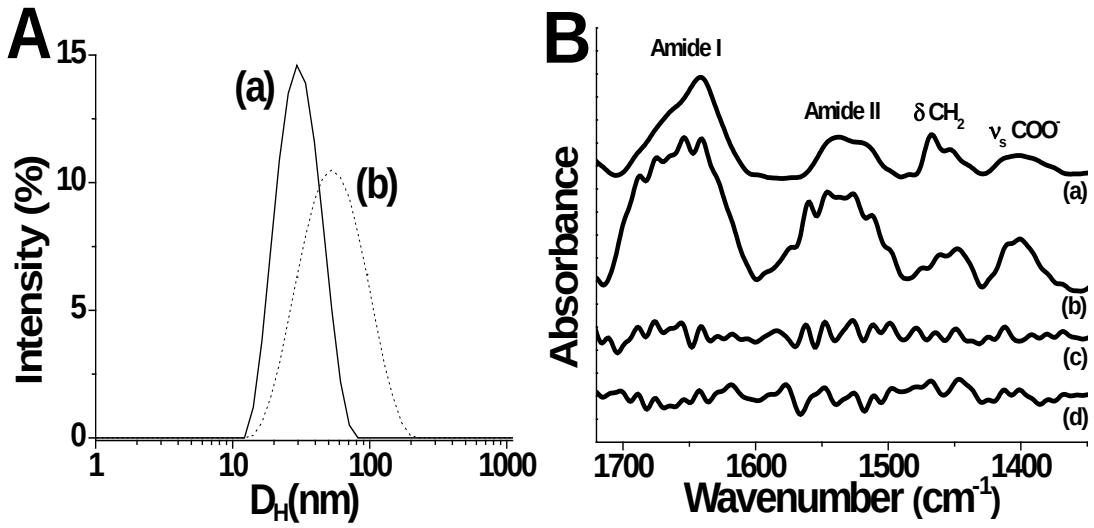


Figure S-11. (A) Dynamic light scattering results showing an increase in hydrodynamic size for the bare Au NPs (a) after conjugation with rituximab (b). (B) Fourier-transform infrared spectra for rituximab-Au NP conjugates (a), rituximab (b), the supernatant of the rituximab-Au NP conjugates after centrifugation (c), and citrate stabilized Au NPs (d). Evidence for conjugation was provided by the presence of protein amide I and amide II bands in the Fourier-transform infrared spectrum of rituximab modified Au NPs (a). Similar bands were obtained in the spectra of rituximab (b), but not for the bare Au NPs (d), nor for the supernatant of the centrifuged rituximab-Au NP conjugates (c).

X. Glycoanalysis of rituximab: Visual Evidence

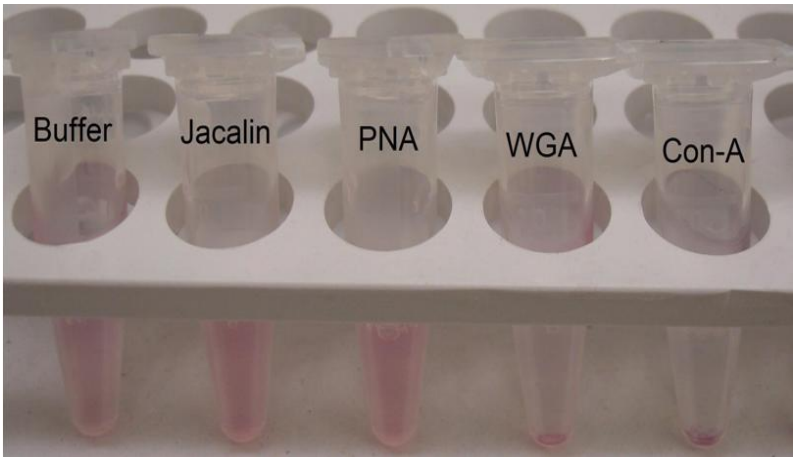


Figure S-12. Photo shows that rituximab-Au NP conjugates solutions retain their typical red-pink color after 24 hours in buffer or in the presence of the control lectins jacalin and PNA. Sedimentation of the aggregates formed between the binding lectins (WGA and Con A) and the rituximab-Au NP conjugates can be observed after 24 hours.

REFERENCES

Brewer SH, Glomm WR, Johnson MC, Knag MK, Franzen S. 2005. Probing BSA binding to citrate-coated gold nanoparticles and surfaces. Langmuir 21(20):9303-9307.

Calabretta M, Jamison JA, Falkner JC, Liu Y, Yuhas BD, Matthews KS, Colvin VL. 2005. Analytical Ultracentrifugation for Characterizing Nanocrystals and Their Bioconjugates. Nano Letters 5(5):963-967.

Schuck P. 2000. Size-Distribution Analysis of Macromolecules by Sedimentation Velociy Ultracentrifugation and Lamm Equation Modeling. Biophysical Journal 78:1606-1619.

Thomas GB, Rader LH, Park J, Abezgauz L, Danino D, DeShong P, English DS. 2009. Carbohydrate Modified Catanionic Vesicles: Probing Multivalent Binding at the Bilayer Interface. Journal of the American Chemical Society 131(15):5471-5477.

Tsai DH, Zangmeister RA, Pease LFI, Tarlov MJ, Zachariah MR. 2008. Gas-Phase Ion-Mobility Characterization of SAM-Functionalized Au Nanoparticles. Langmuir 24:8483-8490.